Surgical Simulation Robot with Haptics and Friction Compensation

Tao Yang[1(✉)], Weimin Huang[1], Kyaw Kyar Toe[1], Jiayin Zhou[1], Yuping Duan[1], Yanling Chi[1], and Loong Ee Loh[2]

[1] Institute for Infocomm Research, Singapore 138632, Singapore
{tyang,wmhuang,kktoe,jzhou,duany,ylchi}@i2r.a-star.edu.sg
[2] School of Mechanical and Aerospace Engineering,
Nanyang Technological University, Singapore 639798, Singapore
leloh1@e.ntu.edu.sg

Abstract. Haptic feedback brings a surgical simulator closer to real surgery. However, friction in surgical simulator's hardware affects its performance significantly. We introduce a surgical simulation robot with roller mechanism for laparoscopic surgical simulation. Roller mechanism is implemented in a constrained space to reduce the friction. Motion based friction cancellation method is also applied to further mitigate the friction effects. Comparing with the same surgical simulation robot without roller mechanism, the one with roller mechanism reduces friction by 32.86 % and 38.87 % on two motion directions, and the motion based friction cancellation method can mitigate the friction effect by 49.46 % and 62.08 % on the two motion directions.

Keywords: Laparoscopic surigcal simulator · Haptics · Friction compensation

1 Introduction

In a laparoscopic surgery, the surgeon has limited access, i.e. visual and haptic only, to the pathological site. The tactile feeling provides the information not only on anatomy, but also on the pathology and the insertion depth of the MIS (Minimally Invasive Surgery) instruments. The tactile information conveys the tool-tissue interaction status to the surgeon through the sense of touch. It always plays an important role in decision making during the surgery [1]. The training instructor also teaches the medical residents to perceive the tactile information during training. Nowadays, as the advent of computer, robotics and virtual reality technologies, various types of simulators and robot assisted devices have been developed for the purpose of laparoscopic surgical training. Most of the surgical simulators or robot assisted surgery tools [2–5] are designed with haptic output capability that enables the system to give the user tactile feelings.

The haptic function built in the surgical simulator or robot is a force output function of the system that simulates the tool-tissue interaction, although there is

X. Luo et al. (Eds.): CARE 2015, LNCS 9515, pp. 69–80, 2016.
DOI: 10.1007/978-3-319-29965-5_7

no real tool-tissue interaction under the handheld devices. In our previous work [6], a laparoscopic surgical simulation robot was studied. We applied a semi-spherical mechanism to execute trajectory and haptics for a virtual laparoscopic surgery. There are lots of moving parts contacting with each other in the robot. Hence, friction is inevitable in such systems, which affects the performance of the robot in moving, positioning and torque delivery etc. It needs to be taken care of when considering a stable haptic output, especially for high haptic output at low velocity. Two basic methodologies are commonly applied to deal with friction, i.e. minimize the friction by design and mitigate the friction by compensation. Unfortunately, friction forces are highly non-linear. It is difficult to compensate. Therefore, it is important to reduce the friction forces by designing the system mechanism and apply appropriate compensation technology to mitigate the effect of remaining friction. Friction compensation methods have been studied thoroughly in the past decades [7,8], such as fixed friction compensation, model-based compensation, and neural fuzzy techniques. Neural network method is one of the good methods for friction compensation in practical engineering, as the neural network is capable to handle highly non-linear scenarioes [9]. However, neural network solution is not a physical based method where the parameters do not relate to the physical phenomena directly. Various friction models have been proposed and tested to understand and compensate the frictional force. Most friction models could not match with the real friction scenarios well after a long service period due to wear and tear.

In this paper, a new robot design for laparoscopic surgical simulation is presented. We apply both design and compensation techniques to reduce friction and mitigate its effects respectively. Friction forces in between the moving parts are reduced by introducing teh roller mechanisms. A motion based friction cancellation method with friction model is applied to mitigate the friction effect for stable haptic output. The paper is organized as follow: Sect. 2 describes the low friction design, finite element analysis and system modelling of the semi-spherical mechanism for the surgical simulation robot. Section 3 describes the motion based friction compensation method and its application on the robot. The work is concluded in Sect. 4.

2 Surgical Simulation Robot

2.1 Friction in Haptics

A surgical simulation robot, as shown in Fig. 1 was designed for image guided robot assisted surgical training in our previous work [6]. The replicated surgical tools are driven by the robot to allow the user to operate on virtual patient with haptic feedback, and provide haptic guidance for surgical training purpose as well. Each of the replicated laparoscopic surgical tools has five Degree-of-Freedom (DOF), namely pitch, yaw, translation, roll and handle grasping. It mimics the DOF of surgical tools in real laparoscopic surgery. A semi-spherical mechanism is the major component to achieve the DOFs mentioned above [6]. Friction in the semi-spherical mechanism affects the performances of haptics, especially the friction on pitch and yaw axes.

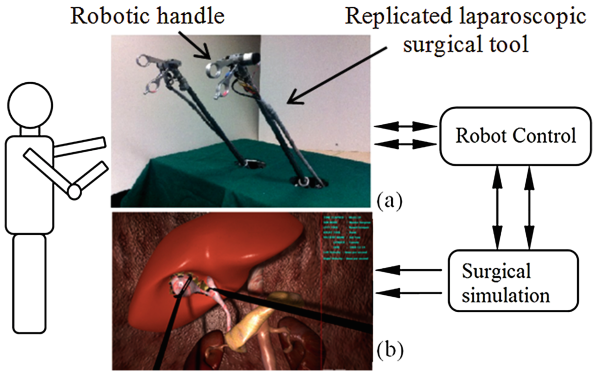

Fig. 1. Overview of the surgical training system: (a) robotic surgical trainer and (b) virtual surgical simulation platform.

As experienced in our robot, friction is inevitable, and it is highly non-linear and difficult to model. It can be categorized as two basic categories, the rolling friction and the sliding friction. The rolling friction is expressed as

$$F_r = C_{rr} F_N, \tag{1}$$

and the sliding friction is expressed as

$$F_s = \mu F_N, \tag{2}$$

where C_{rr} is the rolling resistance coefficient which depends on material elasticity, μ is the sliding friction coefficient which depends on material pair and surface condition. μ is usually much larger than C_{rr}, F_N is the normal force acting on the contact surface. In a haptic device, it can be expressed as a function of haptic output.

2.2 Design Considerations

We introduce a bearing-like mechanism to create rolling motion on the semi-spherical mechanism to reduce friction and enhance the haptic performance. Figure 2(a) shows the overall design of a semi-spherical mechanism with rollers that reduces the frictional force. The semi-spherical mechanism can be divided into four parts as shown in Fig. 2(b). Part I and Part II contain guiding blocks where the rollers are hosted. Part III includes two arches clamped in between of Part I and Part II. Part IV applies and maintains appropriate pressure in between of Parts I and III, Parts II and III. Hence, the mechanical gap between the rollers and Part III, and the motion precision of Part I could be controlled.

Rollers were placed at all possible places, as shown in Fig. 2(a) where relative motion exists. Due to space constraint, the rollers were supported by bushings instead of ball bearings. The relative motion between the roller and its hosting bush still introduces sliding friction. Polytetrafluoroethylene (PTFE) was

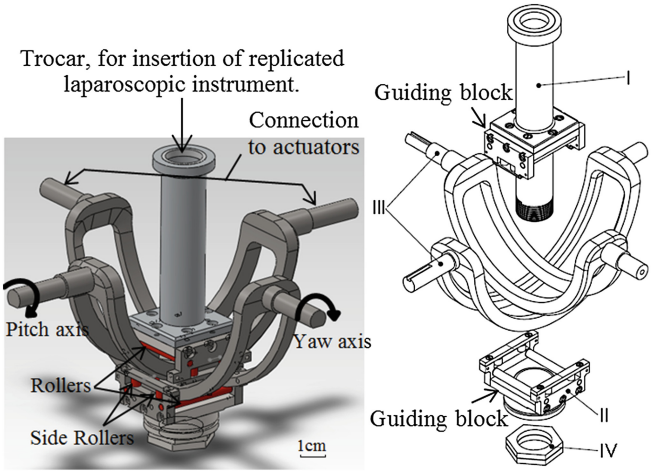

Fig. 2. (a) Overall view of semi-spherical mechanism that provides lower friction for haptic output. (b) Four major components. I: upper guiding block with rollers, II: lower guiding block with rollers. III: two arches which work as haptic input/output interface for pitch and yaw axes. IV: locking nuts for adjusting proper pressure between part I, II and III.

selected to work as bushing for its low friction coefficient and high wear resistance. Although PTFE has very good wearing resistance, it would still be worn off and the size of the hole will be changed where the roller is hosted. However, the contacting profile between the roller and the bushing would not be altered significantly, and hence the friction profile. With this design, wear and tear on the rollers and their contacting surfaces are minimized. The contact profile between the roller and the contact surface could be maintained consistent even after a long service period.

2.3 FE Analysis

The finite element analysis by Abaqus/Explicit 6.13 was adopted to investigate the stress distribution of the semi-spherical mechanism design under loading along pitch and yaw axes (x and y directions in Cartesian coordinate, as shown in Fig. 3). Fifty Newton was applied at a reference point (RP) which is on the trocar's longitudinal axis and 300 mm (equivalent to 15 Nm) above rotational origin of the axis. The translational DOFs of each node on the trocar were coupled with those of the RP to simulate a surgical tool passing through the trocar. Quasi-static loading procedure was applied in the analysis. The two arches were modeled as rigid body and were fully fixed at their reference points as shown in Fig. 3.

The material properties of the components in the mechanism are listed in Table 1. The friction coefficient was 0.16 between steels and 0.05 between steel

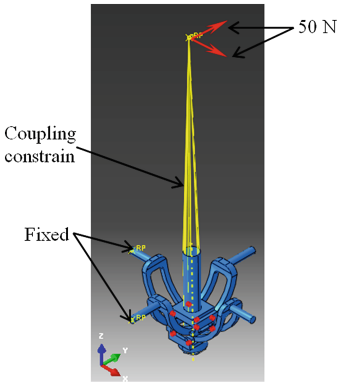

Fig. 3. FE modelling of the semi-spherical mechanism.

Table 1. Material properties used in FE model

	Density(kg/m^3)	Young's modulus(GPa)	Poisson's ratio
Stainless steel	7850	200	0.3
PTFE	2600	0.55	0.46

and PTFE. The trocar was meshed with shell element S4R and the rest components were meshed with solid element C3D4.

Under loading along yaw axis, the maximum Von Mises stress is around 15 MPa at the roller, as shown in Fig. 4. When loading along pitch axis, the rollers also have similar stress distribution with a maximum stress around 12 MPa. Under loading along pitch axis, the maximum Von Mises stress, around 70 MPa, occurs at two side rollers. Under both pitch and yaw loadings, the two guiding blocks of the rollers have small stress level. Figure 5 shows the stress distribution of the guiding block under loading along yaw axis, the Von Mises stress is around 1–2 MPa for the shaft of the side rollers.

The simulation results show that the maximum stress is far below the yield stress of the stainless steel when it is loaded at 15 Nm torque. It suggests that the strength of the semi-spherical mechanism is sufficient for haptic output. The semi-spherical mechanism was fabricated as shown in Fig. 6.

2.4 System Modelling

The semi-spherical mechanism was installed in an existing robot control system [6] to connect with actuators and inserted with a replicated laparoscopic surgical tool. A frequency response experiment was conducted to measure the system response. We assume that the data acquisition speed of a force sensor in the haptic feedback loop is infinitely high, hence the haptic output force is proportional to the acceleration of the surgical tool by $F = ma$, where m is a

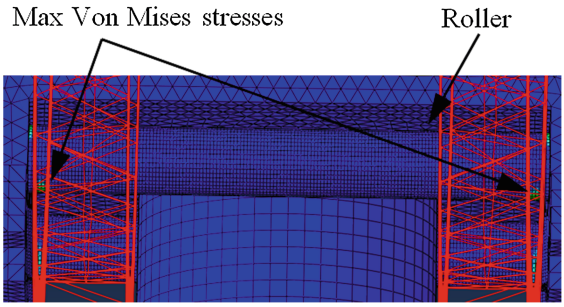

Fig. 4. Locations of maximum Von Mises stresses when the mechanism is under loading along yaw axis.

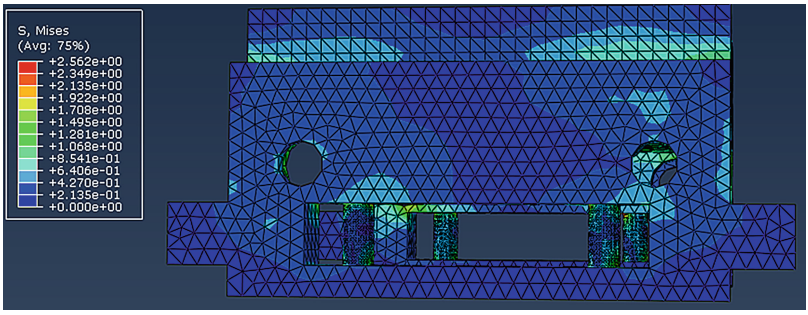

Fig. 5. Stress distribution of the guiding block under loading along yaw axis.

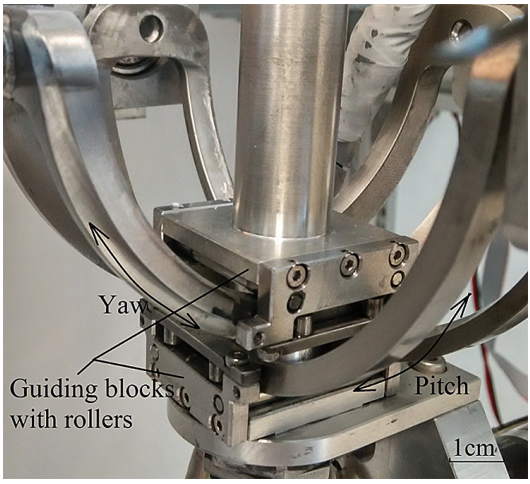

Fig. 6. Fabricated semi-spherical mechanism with rollers, and relative velocity at the contacting area of each axis.

mass constant. Therefore we can use the transfer function of system acceleration to represent the transfer function in haptic force. The transfer function for the robot can be obtained by dividing the measured acceleration $\alpha_m$with the commanded acceleration α_c,

$$G = \frac{\alpha_m}{\alpha_c}. \tag{3}$$

Sinusoid signal with frequency up to 20 Hz was input to the robot. Figure 7 shows the bode plot obtained from the experiment data.

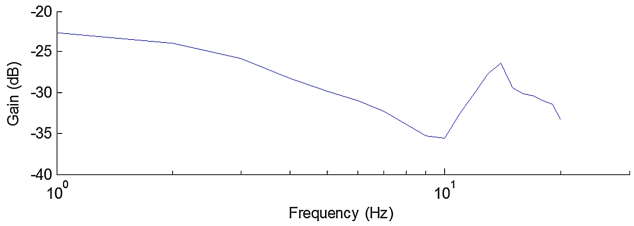

Fig. 7. Open loop bode plot of the semi-spherical mechanism with a replicated surgical tool.

The robot system was taken as second order system. Matlab system identification toolbox was applied to model the system based on the open loop bode plot shown in Fig. 7. The system transfer function $G(s)$ is estimated as

$$G(s) = \frac{0.03s + 0.06}{s^2 + 0.18s + 0.0064}. \tag{4}$$

3 Friction Control Model for Haptics

Despite of the design considerations for friction reduction, friction compensation is still required as high haptic output will lead to high frictional force between the moving parts. The resultant frictional force in the design is a combination of sliding friction from the bushings and rolling friction from the rollers. Hence, stribeck phenomena would affect the performance of haptic output, especially when the haptic output force is large and moving velocity is low.

Experiments were conducted to measure the frictional force with respect to the velocity and haptic output. The robot was set to output a series of haptic force exerting on a user. The haptic output was set from 1 N to 7 N with 1 N increment for each experiment. The user pushed the robotic handle (as shown in Fig. 1) to move against the direction of haptic output. The guiding block with rollers moved from one end of the arch to the other end as shown in Fig. 6. The force applied to execute the motion was measured while the robotic handle was moving. Frictional force was obtained by subtracting the desired haptic output from the measurement. This procedure was repeated 50 times at each haptic

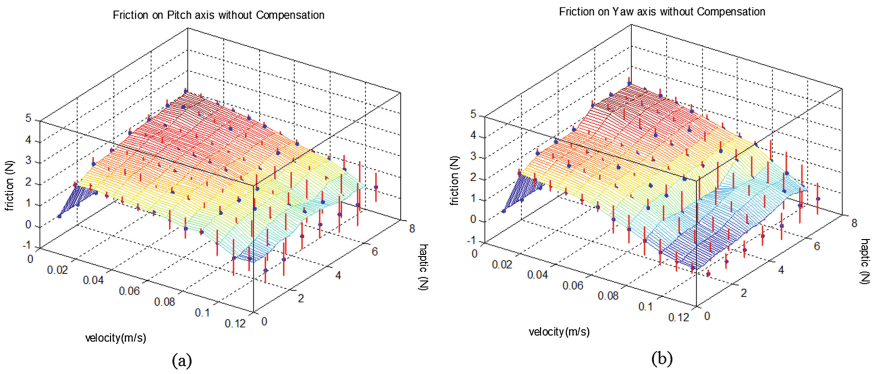

Fig. 8. Mean frictional force from current design with haptic output from 1 N to 7N. The frictional force is larger when the components are just to move, and it is reduced significantly and tends to stabilize when the components moving at higher velocity. The frictional forces are generally higher when the robot outputs a higher haptic force. Vertical bars are the standard deviations at the specific velocity and haptic output. (a) Frictional force for pitch axis. (b) Frictional force for yaw axis.

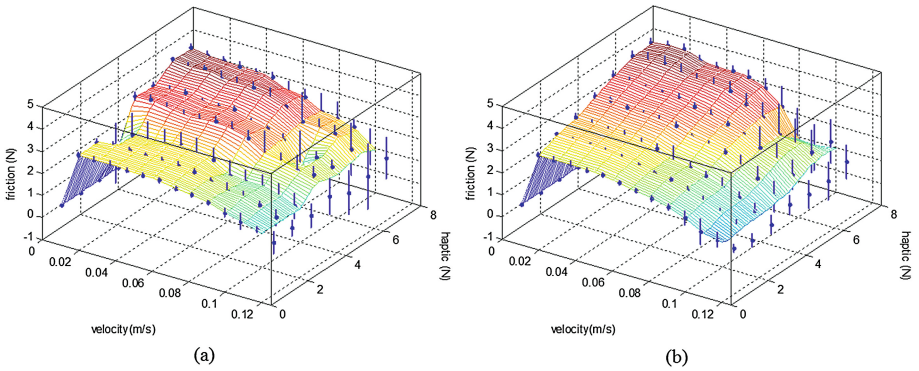

Fig. 9. Mean frictional force measured from the design in [6]. Vertical bars are the standard deviations at the specific velocity and haptic output. (a) Frictional force for pitch axis. (b) Frictional force for yaw axis.

level. The velocity span covered from 0 to 0.125 m/s. The maximum velocity in the experiment was relatively low. Therefore, viscous friction was not taken into consideration during modelling.

Figure 8 shows the measured frictional force on both moving axis. The overall haptic output is smooth, and the maximum friction forces are 2.79 N and 2.98 N for pitch and yaw axes respectively. These measurements will be used in fitting with friction model for compensation. The same experiment was conducted on our previous design in [6] to measure the frictional force. The design has similar overall structure, but no roller mechanism. All moving components create sliding friction. The measured friction forces are shown in Fig. 9. The maximally friction

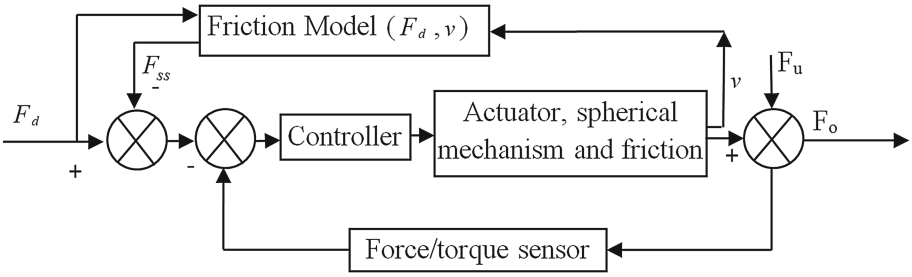

Fig. 10. Control diagram for friction compensation and haptic output. F_d is the haptic output reference force or the desired haptic output, F_o is the haptic output force, F_u is the user's interaction force.

forces are 3.96 N and 4.13 N for the pitch and yaw axes respectively. Comparing Figs. 8 and 9, we notice that the overall friction forces with the design are reduced by 32.86 % and 38.87 % on pitch and yaw axes respectively when comparing with the mechanism without rollers in the same velocity and haptic output span.

Here, we applied a motion based friction cancellation method to compensate the effect of friction and the stribeck phenomena for stable haptic output. The control diagram of such haptic output system is shown in Fig. 10.

Various friction models have been proposed by researchers [10]. A basic friction model was employed in this study. The friction model is written as

$$F_{ss} = (F_c + (F_s - F_c)e^{-(v/v_s)^2})sgn(v), \tag{5}$$

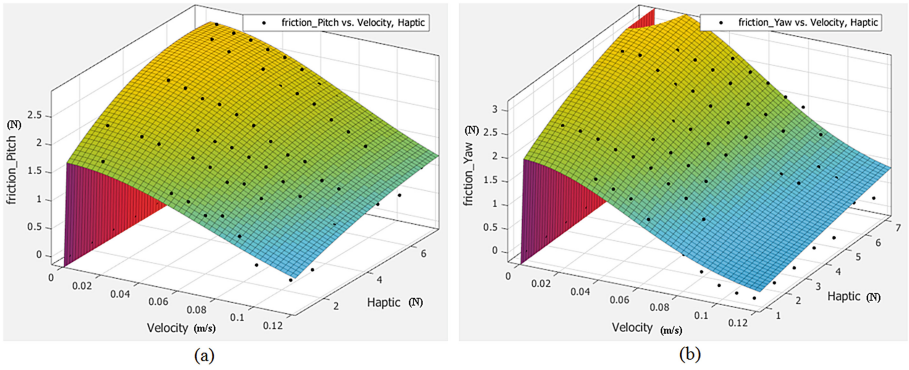

Fig. 11. Surface fitting result with Eq. 5. Experimental results shown in Fig. 8 were fitted with Eq. 5 using Matlab curve fitting toolbox. Black dots are the down sampled experimental measurements. (a) Frictional force fitting for pitch axis with $\mu_e = 0.08$, $a_2 = -0.032$, $a_1 = 0.403$, $a_0 = 1.476$. (b) Frictional force fitting for yaw axis with $\mu_e = 0.086$, $a_2 = -0.019$, $a_1 = 0.351$, $a_0 = 1.82$.

where F_{ss} is the steady state friction, F_c is the Coulomb frictional force, F_s is the stribeck force, v_s is the relative velocity at stribeck, v and is the relative velocity of two moving components. F_c and F_s are dependent on the magnitude of haptic output. They can be written as a function of the desired haptic output F_d, i.e. $F_c = f_c(F_d)$, $F_s = f_s(F_d)$. The functions need to be determined experimentally as different system configuration results in different friction profile. For the semi-spherical mechanism with rollers presented in this paper, the Coulomb frictional force was taken as

$$F_c = \mu_e F_d, \tag{6}$$

where $\mu_e$is an equivalent friction coefficient for the system. A second order polynomial function is taken to represent the stribeck force as

$$F_s = a_2 F_d^2 + a_1 F_d + a_0 \tag{7}$$

Curve fitting was applied on the experiment data (shown in Fig. 8) to identify the parameters in Eqs. (5), (6) and (7). Figure 11 and Table 2 show the surface fitting results and the estimated parameters.

The motion based cancellation method was tested by the same experiment method described in the beginning of Sect. 3. Figure 12 shows the mean frictional force measured from pitch and yaw axes. Comparing with frictional force shown in Fig. 8 in which has no compensation, the frictional force and the stribeck

Table 2. Frictional force fitting results with Eq. (5).

	R^2	Adjusted R^2	RMSE
Pitch	96.75 %	96.65 %	0.14
Yaw	93.92 %	93.72 %	0.24

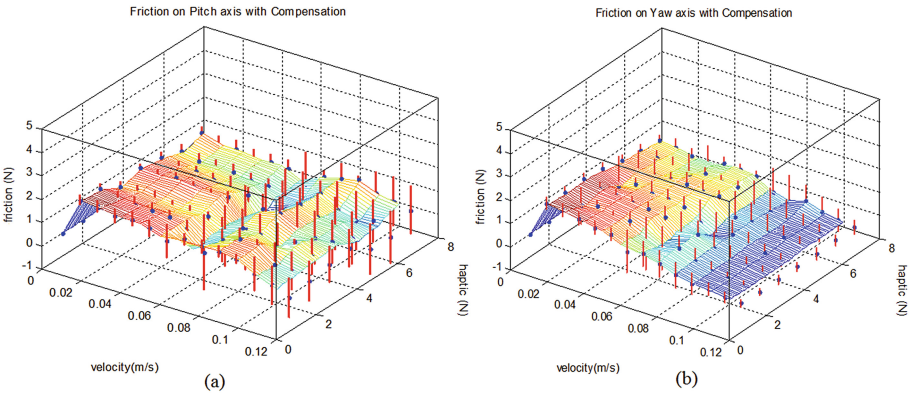

Fig. 12. Mean frictional force measured with friction compensation. Vertical bars are the standard deviations at the specific velocity and haptic output. (a) Frictional force for pitch axis. (b) Frictional force for yaw axis.

phenomena have been mitigated significantly. The total volume covered under the surface (Fig. 12) were reduced by 49.46 % and 62.08 % for pitch and yaw axes respectively. The max measured friction is about 1 N whereas it could reach to 2.5 N when there is no compensation. Figure 12 suggests that the motion based cancellation method is able to work well with a wide range of velocity on our designed mechanism, from 0.02 m/s to 0.12 m/s. It is noticed that the standard derivations increase slightly when the velocity is higher. Comprehensive system model and friction model are required to further improve the performance of this motion based cancellation method.

4 Discussion and Conclusion

A design for laparoscopic surgical simulation robot was presented in this work. Design consideration, FEM verification, system modelling, friction identification and compensation were studied. The semi-spherical mechanism with rollers reduces frictional force significantly comparing to the mechanism without rollers. The motion based cancellation method is capable to mitigate the effect of friction well. Although the frictional force has been mitigated significantly, some residual friction forces are still not removed. It is due to the limitation of motion based cancellation method, which needs a velocity input before the friction model can estimate the frictional force for compensation, but the frictional force is already there before velocity is detected. The compensation is therefore always delayed. Advanced friction compensation methods thus need to be explored to further improve the performance.

Acknowledgments. This work is supported by Agency for Science, Technology and Research, Singapore.

References

1. Ottermo, M.V., Ovstedal, M., Lango, T., Stavdahl, O., Yavuz, Y., Johansen, T.A., Marvik, R.: The role of tactile feedback in laparoscopic surgery. Surg. Laparosc. Endosc. Percutan. Tech. **16**, 390–400 (2006)
2. Hyosig, K., Wen, J.T.: Robotic assistants aid surgeons during minimally invasive procedures. IEEE Eng. Med. Biol. Mag. **20**, 94–104 (2001)
3. van den Bedem, L.J.M., Hendrix, R., Naus, G.J.L., van der Aalst, R., Rosielle, P.C.J.N., Nijmeijer, H., Maessen, J.G., Broeders, I.A.M.J., Steinbuch, M.: Sofie, a robotic system for minimally invasive surgery. In: The 6th International MIRA Congress, Athens, Greece, p. 056 (2011)
4. van den Bedem, L.J.M.: Realization of a demonstrator slave for robotic minimally invasive surgery/door Linda Jacoba Martina van den Bedem. In: Department of Mechanical Engineering. Doctoral degree Technische Universiteit Eindhoven, p. 199 (2010)
5. Simbionix (2014). http://simbionix.com/simulators/lap-mentor/

6. Yang, T., Liu, J., Huang, W., Su, Y., Yang, L., Chui, C.K., Ang Jr., M.H., Chang, S.K.Y.: Mechanism of a learning robot manipulator for laparoscopic surgical training. In: Lee, S., Cho, H., Yoon, K.-J., Lee, J. (eds.) Intelligent Autonomous Systems 12. AISC, vol. 194, pp. 17–26. Springer, Heidelberg (2013)
7. Olsson, H., Astrom, K.J., Canudas de Wit, C., Gafvert, M., Lischinsky, P.: Friction models and friction compensation. Eur. J. Control **4**, 176–195 (1998)
8. Bona, B., Indri, M.: Friction compensation in robotics: an overview. In: 44th IEEE Conference on Decision and Control, and 2005 European Control Conference, CDC-ECC 2005, pp. 4360–4367 (2005)
9. Nguyen, D.H., Widrow, B.: Neural networks for self-learning control systems. IEEE Control Syst. Mag. **10**, 18–23 (1990)
10. Armstrong-Hlouvry, B., Dupont, P., De Wit, C.C.: A survey of models, analysis tools and compensation methods for the control of machines with friction. Automatica **30**, 1083–1138 (1994)